Ferroelectrics, 1991, Vol. 118, pp. 411–424
Reprints available directly from the publisher
Photocopying permitted by license only

OPTICAL ABSORPTION COEFFICIENT AND NON-RADIATIVE QUANTUM EFFICIENCY PHOTOPYROELECTRIC SPECTRA OF PURE CRYSTAL SILICON FROM A SINGLE MODULATION FREQUENCY

C. CHRISTOFIDES, A. ENGEL and A. MANDELIS

Photoacoustic and Photothermal Sciences Laboratory, Department of Mechanical Engineering, and Ontario Laser and Lightwave Research Center, University of Toronto, Toronto, Ontario, Canada M5S 1A4

(Received April 22, 1990, in final form August 1, 1990)

In this work we present and analyze photopyroelectric experimental data obtained for pure crystalline silicon by a novel, compensating differential photopyroelectric spectrometer. The measurements were performed as a function of wavelength (1000–1400 nm) and modulation frequency (15 to 275 Hz). The experimental results will be discussed in the light of an existing photopyroelectric model and in terms of well established semiconductor silicon physics. We illustrate, for the first time, the possibility of extracting the optical-absorption-coefficient and the non-radiative quantum efficiency spectra self-consistently, by using only one experimental photopyroelectric spectrum at a single modulation frequency.

I. INTRODUCTION

As is well known, the optical absorption coefficient and the non-radiative quantum efficiency of semiconductors are of major interest because they provide information regarding the density and spectral activity of defect states in the material, particularly below the bandgap energy.

Photopyroelectric spectroscopy (P^2E), as pointed out elsewhere[1,2] has a certain number of advantages when the optical absorption coefficient is very small, for instance, as is the case, below the bandgap energy of semiconductors.[1] As pointed out before,[2–5] the main advantage of P^2ES over other conventional photothermal spectroscopies is the fact that one can measure directly and self-consistently the optical absorption coefficient, $\beta(\lambda)$, and the non-radiative quantum efficiency, $\eta(\lambda)$, spectra.

Mandelis *et al.*[4] and Christofides *et al.*[5] have shown the possibility of using the photopyroelectric technique to find the optical absorption coefficient, $\beta(\lambda)$, and the non-radiative quantum efficiency, $\eta(\lambda)$, spectra of *a*–Si:H and Ge semiconductors, respectively. These authors have shown that high-modulation-frequency data (thermally thick limit), yielded the optical-absorption-coefficient spectrum, while at low modulation frequencies (thermally thin limit), the non-radiative quantum efficiency spectrum was obtained self-consistently by substitution of the experimental optical absorption coefficient spectrum to the thermally thin limit photopyroelectric theory.[6]

The distinction of two modulation frequency regimes (thin and thick limits) led to the simplification of the general mathematical photopyroelectric model and also

to a simplification of the analysis.[6] Unfortunately the simplification of the mathematical analysis by the distinction of two thermal regimes is not always possible, but is strongly dependent on the thickness and thermal properties (e.g. thermal diffusivity) of the sample under investigation. It is also important to note that sometimes it is difficult to define the frequency limits for purely thermally thin or thick conditions. In order to avoid these problems, we plan to consider the global equation which expresses the photopyroelectric signal with a limited number of simplifications.

The aim of this paper is to demonstrate the evaluation of $\beta(\lambda)$ and $\eta(\lambda)$ for pure, crystalline silicon from only one photopyroelectric spectrum, at a single frequency which is within the sample thermally thin limit; otherwise $\eta(\lambda)$ is not separately obtainable. The means of attaining this goal is by use of the real (in-phase) and imaginary (quadrature) parts of the photopyroelectric signal, and formation of a system of two simultaneous equations with two unknowns [$\beta(\lambda)$ and $\eta(\lambda)$]. The experimental results will be discussed according to the photopyroelectric theory developed by Mandelis and Zver[6] without any simplifications of the model and in terms of well-established silicon properties. Toward this end, a single P^2E spectrum has been recorded and introduced into the global mathematical photopyroelectric equation, in order to obtain $\beta(\lambda)$ and $\eta(\lambda)$ from the same modulation frequency.

II. THEORETICAL MODEL

Figure 1 presents a one-dimensional geometry of the photopyroelectric system. A solid sample (Si in our case), of thickness L_s, is irradiated by monochromatic light of wavelength λ, whose intensity is modulated at frequency f. If the pyroelectric

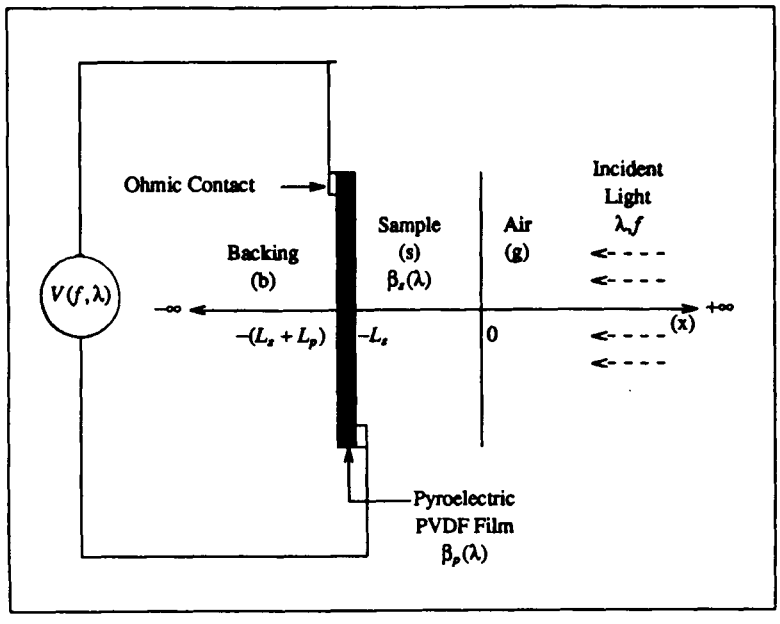

FIGURE 1 One-dimensional geometry of a photopyroelectric system.

film is optically opaque and thermally thick, and the surface reflectance is included in the form $A_s = 1 - R_s$, then the photopyroelectrically detected voltage is given by the relation[6]:

$$V[f,\beta_s(\lambda),\eta_s(\lambda)] = \frac{pI_oA_s}{2k\varepsilon_o}\left\{\left(\frac{\beta_s\eta_s}{k_s(\beta_s^2 - \sigma_s^2)\sigma_p}\right)[2(b_{sg}r_s + 1) - [(r_s + 1)(b_{sg} + 1)\exp(\sigma_sL_s) + (r_s - 1)(b_{sg} - 1)\exp(-\sigma_sL_s)] \cdot \exp(-\beta_sL_s)] + \frac{\eta_p\exp(-\beta_sL_s)}{k_p\beta_p\sigma_p}[(b_{sg} + 1)(b_{ps}r_p + 1)\exp(\sigma_sL_s) + (b_{sg} - 1)(b_{ps}r_p - 1)\exp(-\sigma_sL_s)]\right\} \div [(b_{sg} + 1)(b_{ps} + 1)\exp(\sigma_sL_s) + (b_{sg} - 1)(b_{ps} - 1)\exp(-\sigma_sL_s)] \quad (1)$$

where p and k are the pyroelectric coefficient and the dielectric constant of the pyroelectric medium, respectively; I_o is the light source irradiance incident at the solid surface; ε_o is the permittivity constant of vacuum ($8.85418 \times 10^{-12}\ C/Vm$); and η_s and η_p are the non-radiative conversion efficiencies (or heat conversion efficiencies) for the absorbing solid and the pyroelectric film, respectively. The index $j = g,s,p,b$ refers to the gas, sample, photopyroelectric film, and backing, respectively. Furthermore,

$$\sigma_s = (1 + i)a_j \quad (2.1)$$

with $i^2 = -1$, and a_j is the thermal diffusion coefficient, defined as

$$a_j = \sqrt{\pi f/\alpha_j} = \mu_j^{-1} \quad (2.2)$$

where α_j is the thermal diffusivity and μ_j is the thermal diffusion length of the material (j) at modulation frequency f. The remaining thermal coupling coefficients are defined as[6]:

$$b_{mn} \equiv k_ma_m/k_na_n; \quad k_j\text{: thermal conductivity} \quad (3.1)$$

$$r_j \equiv \beta_j/\sigma_j \quad (3.2)$$

Finally, L_s, β_s and L_p, β_p are the thickness and the optical absorption coefficient of the sample and the pyroelectric film respectively. In the absence of a sample, the P^2E signal $V_R(f)$ generated by a thin-film, blackbody non-reflecting reference directly deposited on the pyroelectric detector can be written in the form:

$$V_R(f) = \frac{pI_o}{2k\varepsilon_o}\left(\frac{1}{k_p\sigma_p^2}\right) \quad (4)$$

upon setting $\eta_s = \eta_R = 1, A_s = 1, R_s = R_R = 0$, and $\sigma_sL_s \ll 1$, in Equation (1).

The general Equation (1) shows explicitly that the complex photopyroelectrically induced voltage, $V(f, \beta_s, \eta_s)$, is directly related to the optical and thermal parameters, and contains the values α_s, $\beta_s(\lambda)$ and $\eta_s(\lambda)$ of the sample under investigation. However, due to the complexity of this equation, the mathematical deconvolution

of the optical absorption coefficient and non-radiative quantum efficiency spectra is usually a difficult task. Unlike earlier work,[4] we are not going to distinguish two modulation frequency regimes. Equation (1) may be separated into real and imaginary parts, in order to have two equations and two unknowns [$\beta_s(\lambda)$ and $\eta_s(\lambda)$]. We can divide Equation (4) into Equation (1) to obtain a normalized P^2E signal with the approximations $b_{sg} >> 1$ ($b_{sg} \approx 2149$), $b_{ps}r_p >> 1$, and $b_{ps} << 1$:

$$V_N[f,\beta_s(\lambda),\eta_s(\lambda)] = A_s(\lambda)b_{ps}\{\eta_s(\lambda)\left[\frac{r_s^2}{r_s^2+1}\left(\frac{2}{e^{\sigma_s L_s}-e^{-\sigma_s L_s}} - \frac{e^{\sigma_s L_s}+e^{-\sigma_s L_s}}{e^{\sigma_s L_s}-e^{-\sigma_s L_s}} + \frac{1}{r_s}\right)\exp(-\beta_s(\lambda)L_s)\right] + \left(\frac{e^{\sigma_s L_s}+e^{-\sigma_s L_s}}{e^{\sigma_s L_s}-e^{-\sigma_s L_s}}\right)\exp(-\beta_s L_s)\} \tag{5.1}$$

and finally Equation (5.1) can be written in terms of hyperbolic functions:

$$V_N[f,\beta_s(\lambda),\eta_s(\lambda)] = A_s b_{ps}\{\eta_s(\lambda)\left(\frac{r_s^2}{r_s^2+1}\left[\frac{1}{\sinh(\sigma_s L_s)} - \left(\coth(\sigma_s L_s)+\frac{1}{r_s}\right)\exp(-\beta_s L_s)\right] + \coth(\sigma_s L_s)\exp(-\beta_s L_s)\} \tag{5.2}$$

By writing the complex factors of Equation (5.2) as:

$$\frac{1}{\sinh(\sigma_s L_s)} = S_R + iS_I \tag{6.1}$$

$$\coth(\sigma_s L_s) = C_R + iC_I \tag{6.2}$$

$$\frac{r_s^2}{r_s^2+1} = r_R + ir_I \tag{6.3}$$

$$\frac{1}{r_s} = r_o(1+i) \tag{6.4}$$

where S_R, S_I, C_R, C_I, r_R, r_I, and r_o are given by Equations (7.1)–(7.8)

$$S_R = \cos(a_s L_s)\sinh(a_s L_s)/D \tag{7.1}$$

$$S_I = -\sin(a_s L_s)\cosh(a_s L_s)/D \tag{7.2}$$

$$C_R = \cosh(a_s L_s)\sinh(a_s L_s)/D \tag{7.3}$$

$$C_I = -\cos(a_s L_s)\sin(a_s L_s)/D \tag{7.4}$$

$$r_R = \frac{\beta_s/a_s^2}{\beta_s/a_s^2+1} \tag{7.5}$$

$$r_I = \frac{(1/2)\beta_s/a_s^2}{\beta_s/a_s^2+1} \tag{7.6}$$

$$r_o = a_s/\beta_s \tag{7.7}$$

D is given by the relation:

$$D = [\cos(a_s L_s)\sinh(a_s L_s)]^2 + [\sin(a_s L_s)\cosh(a_s L_s)]^2 \tag{7.8}$$

By substituting Equations (7.1)–(7.8) into Equations (6.1)–(6.4) and then into Equation (5.1) we can write the general pyroelectric relation as:

$$V_N[f,\beta_s(\lambda),\eta_s(\lambda)] = A_s b_{ps}\{\eta_s(\lambda)(r_R + ir_I)[(S_R + iS_I)((C_R + iC_I) + r_o(1 + i))\exp(-\beta_s L_s)] + (C_R + iC_I)\exp(-\beta_s L_s)\} \quad (8)$$

Equation (8) can then be written:

$$V_N[f,\beta_s(\lambda),\eta_s(\lambda)] = A_s(\lambda) b_{ps}\{\eta_s(\lambda) T_1 + C_1] + i[\eta_s(\lambda) T_2 + C_2]\}, \quad (9)$$

where T_1, T_2, C_1, and C_2 are functions of the optical absorption coefficient:

$$T_1(\beta_s) \equiv (r_R S_R - r_I S_I) - [(r_R C_R - r_I C_I) - (r_o r_R - r_o r_I)]\exp(-\beta_s L_s) \quad (10.1)$$

$$T_2(\beta_s) \equiv (r_R S_I - r_I S_R) - [(r_R C_I - r_R C_R) - (r_o r_I - r_o r_R)]\exp(-\beta_s L_s) \quad (10.2)$$

$$C_1(\beta_s) = C_R \exp(-\beta_s L_s) \quad (10.3)$$

$$C_2(\beta_s) = C_I \exp(-\beta_s L_s) \quad (10.4)$$

Finally, we write the real and the imaginary parts of the photopyroelectric signal equation as:

$$V_N \cos(\Phi_D) = A_s b_{ps}(\eta_s T_1 + C_1) \quad (11.1)$$

$$V_N \sin(\Phi_D) = A_s b_{ps}(\eta_s T_2 + C_2) \quad (11.2)$$

where Φ_D is the phase different between sample and reference:

$$\Phi_D(f) = \Phi_s(f) - \Phi_R(f) \quad (12.1)$$

and, in principle,

$$\Phi_R = \text{constant} = -\pi/2 \quad (12.2)$$

In experimental practice, however, $\Phi_R(f)$ includes all instrumental phase shifts in the P^2E spectrometer and is used as a calibration curve.[5] Thus, by numerical solution of the system of two equations given by Equations (11.1) and (11.2) the optical absorption coefficient and the non-radiative quantum efficiency can be obtained.

III. SPECTROSCOPIC INSTRUMENTATION

Two experimental configurations were used to allow spectroscopic measurements in a wide range of modulation frequencies. In both cases, white light from a 1000 W Xe lamp was passed through a monochromator, housing an infrared-blazed grating with a resolution of 16 nm which was adjusted using a stepping motor (Step motor 2 in Figure 2) under IBM PS/2 computer control, to produce a beam with variable wavelength. The spectral cut-off filters associated with the monochromator were changed automatically using an electromechanical switch. Then, the beam was focused and directed towards the sample or reference detectors. Using an

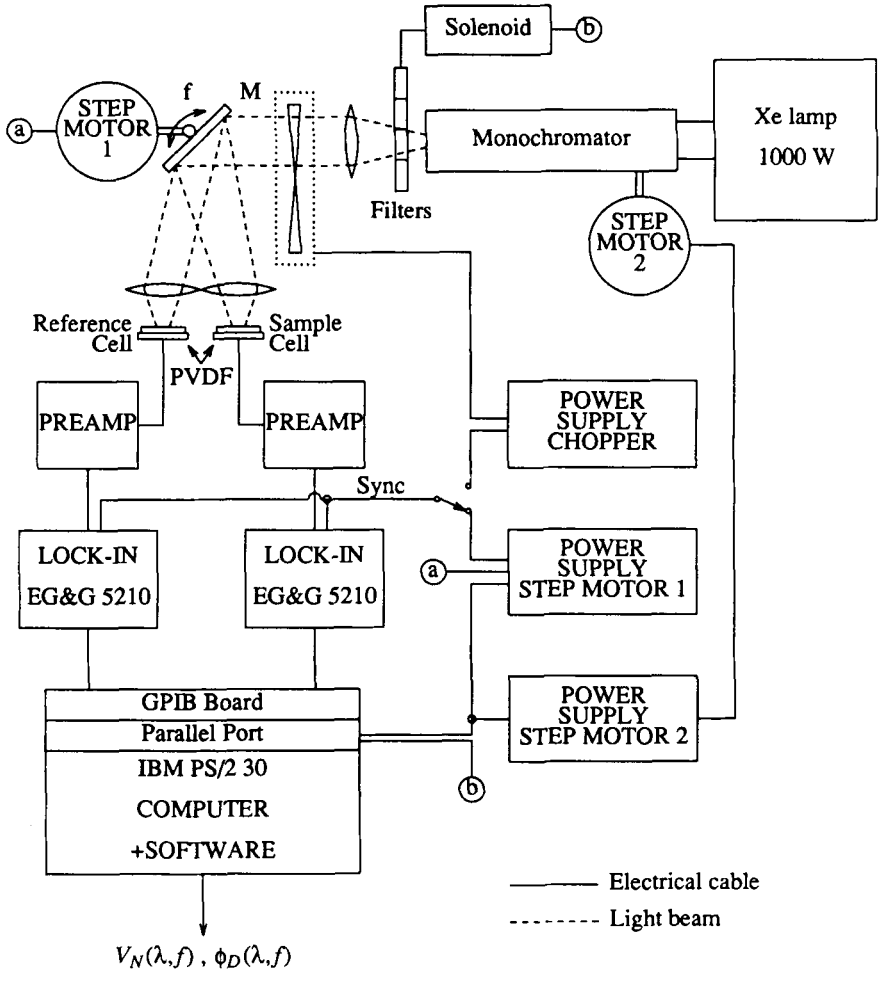

FIGURE 2 Set-up of the photopyroelectric spectrometer.

oscillating mirror (M), the swept beam was alternately focussed on two spots on a plane where the sample and detector would ultimately be placed. At those spots the beam sizes were approximately 1×0.5 mm^2 each in area. A special effort to minimize the size of the illuminated spot was made in order to maximize the irradiance of the incident radiation. The mirror was made to oscillate by a stepping motor (Step motor 1 in Figure 2) in the range of 0.1 to 15 Hz. This modulation method is preferable to a beam splitter-mechanical chopper arrangement, since it avoids the wavelength dependence of such optics. For frequencies in the range of 0.1 to 15 Hz the mirror oscillated automatically to provide modulation. However, for frequencies in the 15–600 Hz range, an EG&G chopper (Model 192) was placed before the mirror to provide the modulation while the mirror was controlled by the computer to switch from the sample to the reference detector, after a measurement at each wavelength was made. In this mode, the data acquisition software ensured that the intensity variation of the lamp during successive measurements of sample and reference did not contribute a considerable error. The two Al–Ni–

PVDF photopyroelectric detectors were covered with black paint in order to absorb maximum optical flux (blackbodies). The two output signals were bandpass-filtered and preamplified by two low noise Ithaco preamplifiers (Model 1201). The two signals were then connected to a double-input Tektronix (Model T912) oscilloscope for visual display, and to two digital EG&G (Model 5210) lock-in analyzers (see Figure 2). Depending on the configuration used, the reference for the lock-ins was obtained either from the oscillating mirror (0.1–1.15 Hz) or from the chopper (15–600 Hz). An IBM computer equipped with a mathematical co-processor for fast calculations interacted with the two lock-ins through a GPIB board, and upon reading their output, it calculated amplitudes and phases. Using only the two black PVDF films the normalized magnitude signal was further calibrated ($V_N \rightarrow 1$) at the beginning of each experiment by a judicious choice of gain on the preamplifiers, before placing the sample on one of the P^2E detectors. Thus, before starting the experiments, any detectable difference between the two photopyroelectric detectors was eliminated by the choice of the preamplifier gains.

The first performed experiments concerned spectrometer characterization. It was observed that the two PVDF detectors ("S": sample and "R": reference) sprayed with black paint, responded nearly ideally to the output light intensity of the Xe lamp: The two responses confirmed that the beams were indeed spectrally similar, and that any apparent differences in intensity could be corrected through the preamplifier gain. These preliminary experiments were performed at various frequencies in the range of 5 to 275 Hz in order to study the effect of modulation frequency on the detector P^2E signal.

For this study, two different thicknesses (28 and 52 μm) of PVDF were tried, in order to obtain thermally thick photopyroelectric conditions. The thickness of the PVDF and the experimental frequency must be such that the condition $a_p L_p \gg 1$ be satisfied, according to the definition of the thermally thick limit:

$$f \gg f_c \equiv \frac{\alpha_p}{\pi L_p^2} \tag{13}$$

where f_c is the critical frequency, for the thermally thin to thick transition, equal to 22 and 5 Hz, for PVDF thicknesses of 28 and 52 μm, respectively. The characterization experiments led to the conclusion that it is necessary to work in a frequency range greater than 5 Hz in order to satisfy the conditions of the theoretical model, which is expressed by Equation (1). For all subsequent experimental work 52 μm-thick PVDF was used in order to allow for the largest range of experimental frequencies, as well as to generate high output voltages. In order to account for the instrumental phase variation, a certain correction via a phase calibration curve was required as a function of the working modulation frequency.

IV. PHOTOPYROELECTRIC SPECTROSCOPIC MEASUREMENTS

For this study, pure c–Si samples with crystalline orientation (100) were used. The samples themselves were squares of dimensions $4 \times 4 \times 0.4$ mm^3. They were

placed on the detector S and gentle pressure was applied in order to have good PVDF-sample contact. Optical measurements have been performed across the bandgap of Si in the range of 1000 to 1400 nm. Figure 3(a) shows normalized P^2E spectra of a Si crystal obtained at various frequencies between 15 and 275 Hz at room temperature. As was expected from the transmission-like nature of the P^2E signal near the bandgap at high frequencies,[6] the normalized P^2E signal amplitude increased with increasing wavelength [see Figure 3(a)]. We note that in the transparent region the signal is higher when the frequency is high. In fact, at low modulation frequencies, when the silicon sample is transparent, the silicon acts as an efficient heat sink, through the boundary with the detector, effectively reducing the magnitude of V_s relative to the reference amplitude V_R, since the reference detector is immersed in air. At higher modulation frequencies the silicon's heat sinking contribution is decreased, as the thermal diffusion length becomes shorter than the thickness of the wafer with a concomitant decrease in thermal energy loss into the gas (air) overlying the sample. Thus, the magnitude of V_s increases relative to the reference signal. Overall, V_N is expected to increase with modulation frequency in the transparent region, but should eventually saturate, and reach a plateau, when the thermally thick limit is attained in the Si sample for thermal flux in its back surface and the magnitude of V_s increases relative to the reference signal. In Figure 3(b) we present Log(V_N) vs. λ in order to be able to resolve the opaque region. In fact the signal in the transparent region was 4 orders of magnitude higher than in the opaque region at 275 Hz and 1.5 orders of magnitude for low modulation frequencies such as at 15 Hz. At short wavelengths, when the modulation frequencies are high, the thermally-thick normalized voltage is very small because in this case the signal depends mostly on the thermal contribution. On the other hand, at low f the P^2E normalized voltage across the bandgap changes less as a function of the wavelength, thus indicating the onset of a certain compensation between the thermal and direct optical transmission contributions.

Figure 4 shows the phase difference Φ_D as a function of the wavelength, λ, for various frequencies at room temperature. These results have been obtained simultaneously with the data presented in Figure 3(a). The following remarks can be made: (1) As was expected in the case of high modulation frequencies, when the bandgap region is approached, Φ_D changes significantly as a function of wavelength, as the photothermal phase lag decreases due to the combined effects of the heat centroid moving closer to the back-surface detector,[7] and the direct transmission signal becoming more significant. The latter effect is important at wavelengths where the sample absorption changes rapidly, *i.e.* across the bandgap. As the modulation frequency is increased, the wavelength at which the "transmission" signal becomes dominant shifts to shorter values, since the absorption related heat centroid signal is attenuated. This effect is experimentally illustrated in Figure 4, as a phase jump occurring at shorter wavelengths when the modulation frequency is increased. (2) At long wavelengths and for all frequencies, all phase difference curves, Φ_D, tend to the same (zero degrees) value, due to the domination of the in-phase direct transmission signal over the photothermal absorption signal. (3) The absolute phase difference Φ_D is greater at higher frequencies, as expected from the theory.[6] The same behavior has already been observed by Christofides *et al.*[5] during photopyroelectric spectroscopic measurements on crystalline Ge.

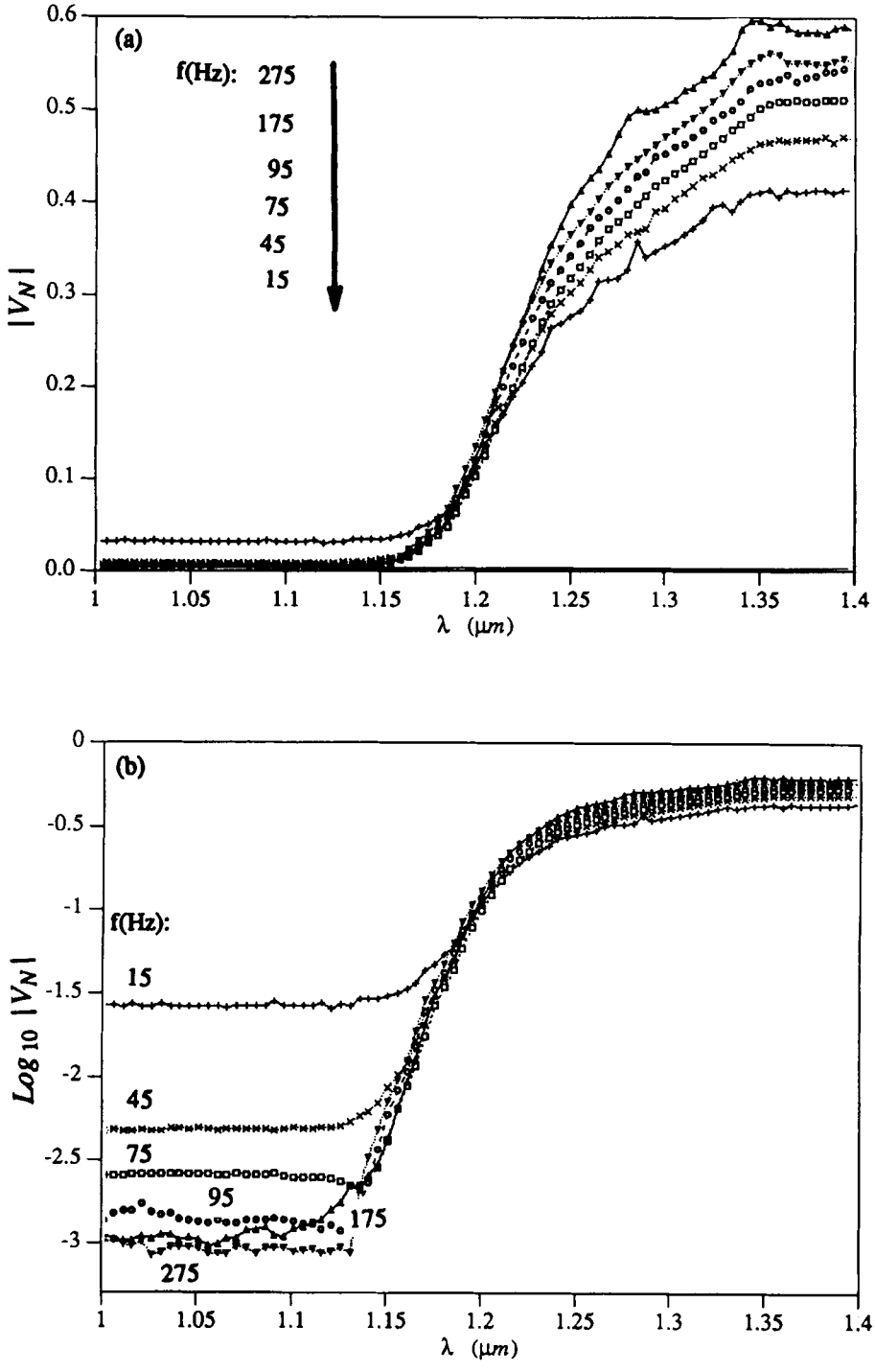

FIGURE 3 (a) P^2E normalized voltage $|V_N|$ spectra of c–Si at the same modulation frequencies. (b) $\text{Log}_{10}|V_N|$ spectra of c–Si at various frequencies.

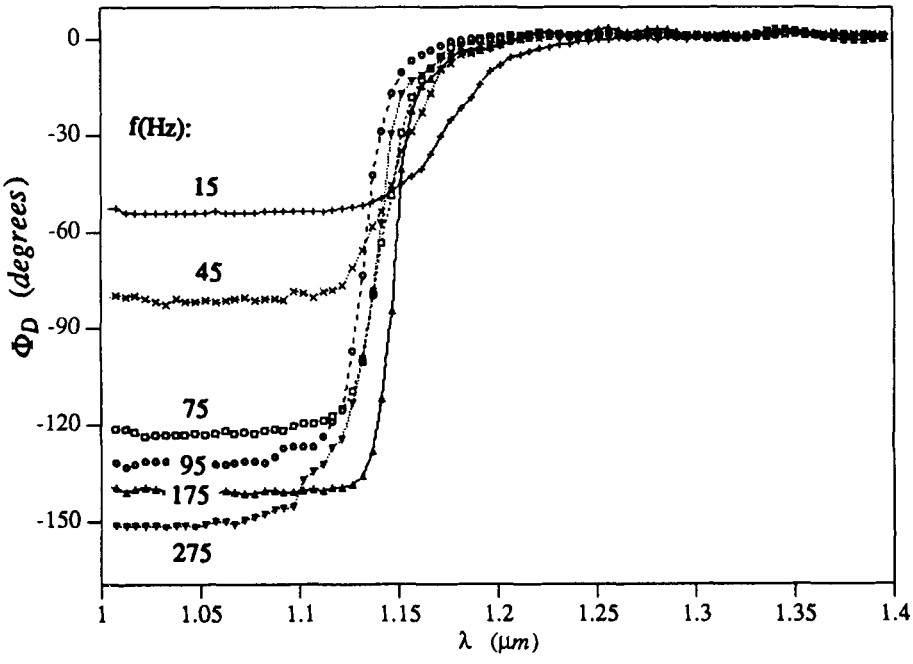

FIGURE 4 P^2E differential phase spectra, Φ_D, of c–Si at various modulation frequencies.

V. DATA ANALYSIS AND DISCUSSION

A. *Optical Absorption Coefficient Spectra*

As stated earlier, one of the targets of this paper is to use the optically compensating P^2E spectrometer to determine the optical absorption coefficient and non-radiative quantum efficiency spectra of a pure crystalline Si sample. We are going to determine $\eta_s(\lambda)$ and $\beta_s(\lambda)$ by using the two photopyroelectric functions given by Equations (11.1) and (11.2). In the case of the photopyroelectric spectroscopic characterization of c-Si wafers, it is impossible to utilize simpler methods, such as the one described by Mandelis *et al.*[4] and Christofides *et al.*[5] using two different modulation regimes. This is so, because the high modulation frequency (thermally thick) regime introduces the condition[6]:

$$L_s >> \mu_s = \sqrt{\frac{\alpha_s}{\pi f}} \tag{14}$$

For silicon wafers (L_s = 0.04 cm), the condition given by the above inequality (for L_s approximately one order of magnitude greater than μ_s), leads to a critical frequency close to 19 kHz, which is experimentally impractical. On the other hand, the low modulation-frequency condition (thermally thin limit) is also not possible to satisfy; the thermally thin limit imposes[7]: $L_s << \mu_s$ which leads to a modulation frequency close to 2 Hz. Technically there is no problem working with such fre-

quencies, however, the theoretical model given in Equation (1) also requires that the working frequency must be greater than 5 Hz, in order for the 52 μm-thick PVDF detector to be thermally thick. In the light of these conflicting requirements, it is easy to understand why Equation (1) or its normalized form as expressed by Equations (11.1) and (11.2) must be used without simplifications, for the quantitative analysis of the experimental results. In Figure (5) we present optical absorption spectra of the c–Si calculated from the 45 Hz and 175 Hz curves of Figures (3) and (4). The mathematical system given by Equations (11) was solved taking from the literature: $A_s = 0.67$,[8] $\alpha_s = 1\ cm^2/s$,[9] and $L_s = 0.04$ cm. The best fit to the data was obtained by using $b_{ps} = 0.35$ which is however four times greater than the one calculated from the value taken from the literature.[9] This may be indicative of imperfect thermal contact at the sample-detector interface. In Figure 5 we note that β_s is nearly independent of the modulation frequency as was expected. $\beta_s(\lambda)$ has been found to be one order of magnitude greater than the one presented in the literature. It seems that the large photopyroelectric signal induced by direct absorption on the PVDF film influences very strongly the absorption coefficient spectrum. In the near future some experimental improvement will be performed in order to increase the quantitative reliability of the technique. In the case of the 15 Hz curve it was noticed however that the derived β_s spectrum was different in the transparent region from spectra derived from other curves in Figure 3. This is expected due to the fact that at 15 Hz, the thermally thick condition imposed by the PVDF films of 52 μm is not entirely satisfied. In fact, 15 Hz is less than one order of magnitude greater than the critical value (5 Hz). According to the experimental results presented in Figure 5, it seems that even at 45 Hz the thermally thick condition is not entirely satisfied. On the other hand, for modulation frequencies 95 and 175 Hz the optical absorption coefficient spectra are identical. As the modulation frequency increases, the short wavelength values of $\beta_s(\lambda)$ approach those presented in the literature[10] except for the photothermal saturation (high-β_s) region.[6] We note a certain disagreement with optical measurements (see

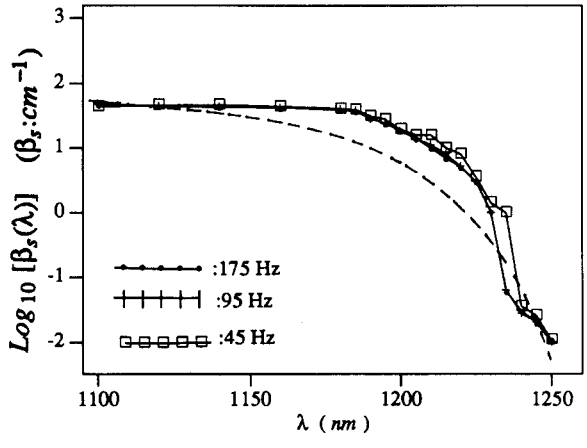

FIGURE 5 Logarithm of the optical absorption coefficient, $Log_{10}\ [\beta_s(\lambda)]$, calculation for Si as a function of the wavelength. Data taken from curves of Figures (3) and (4) at 45, 95, and 175 Hz. Flatness in the short wavelength region is due to photopyroelectric saturation (dashed line from References 8 and 10).

dashed line) in the range between 1100 and 1250 nm.[8] It is believed that the apparent disagreement is due to residual direct absorption by the PVDF sensor. This effect may be corrected using the quadrature method.[11] On the other hand, for wavelengths greater than 1250 nm the solution of the mathematical system given by Equations (11) gives a non-radiative quantum efficiency greater than one, which seems to indicate that in this range the direct absorption of the PVDF film plays an important role.

B. Non-radiative Quantum Efficiency Spectra

Finally, one can determine the non-radiative quantum efficiency spectrum from the system of Equations (11.1) and (11.2). In Figure 6 we present the results obtained from the same P^2E curves that gave Figure 5, at 45, 95, and 175 Hz. We note that in the opaque region η_s is very small. The 95 Hz and 175 Hz spectra are essentially identical. It is seen that η_s increases substantially with a decrease in photon energy below the bandgap. As was mentioned in the previous section, $\eta_s(\lambda)$ for high wavelengths (> 1250 nm) was found to be greater than one which indicates the influence of direct absorption in the PVDF film. Unfortunately, it is impossible to compare these experimental results directly with other data, since the P^2E spectrum in this work gives the first such reported $\eta_s(\lambda)$ spectrum for Si, to the authors' best knowledge. However, two qualitative remarks can be made: (i) $\eta_s(\lambda)$ spectra of Figure 6 anti-correlate with the quantum efficiency spectrum for Si presented by Kirev,[10] as would be expected from complementary electron de-excitation mechanisms (production of free carriers vs. heat generation); (ii) Some results obtained photoacoustically by Kitamura *et al.*[12] using amorphous glass samples $(As_2Se_3)_{100-X}Ge_X$ led to spectral behavior of the non-radiative quantum efficiency across the optical gap qualitatively similar to our study: an increase of $\eta_s(\lambda)$ with increasing λ, below the optical gap of the glass. (iii) Cahen[13] using photoacoustic measurements on a silicon solar cell has shown the dependence of the performance (quantum efficiency) of the cell on the wavelength. That work is

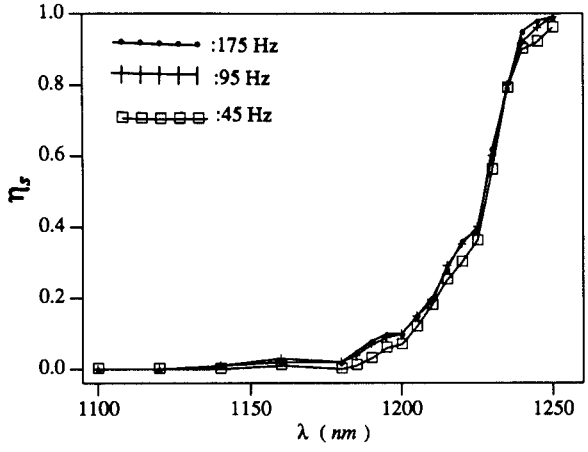

FIGURE 6 Non-radiative quantum efficiency spectrum, $\eta_s(\lambda)$ of crystalline Si obtained from data in Figures (3) and (4) at 45, 95, and 175 Hz.

indicative of the fact that thermalization of free carriers also contributes to non-radiative quantum efficiency yields (and to photothermal signals), without the necessity of the appearance of photoluminescence in electronically active materials. We do feel, however, that the quantitative accuracy of the $\eta_s(\lambda)$ curve is somewhat compromised due to the large photopyroelectric signal induced by the direct absorption of the PVDF film as it was discussed in the comparison of curves in Figure 5 which those found in the literature. (iv) The same behavior has been found for *c*-Ge by the present authors.[5] A more detailed physical analysis of $\eta_s(\lambda)$ spectra is currently under investigation.

VI. CONCLUSIONS

In this paper we presented and analyzed P^2E experimental data obtained for pure crystalline silicon using a photopyroelectric real-time normalizing spectrometer. The experimental photopyroelectric spectra have been used to evaluate the optical absorption coefficient and non-radiative quantum efficiency spectra of pure crystalline silicon. The spectra have been obtained directly and self-consistently from the same P^2E data at one modulation frequency. The ability of the theoretical model presented by Mandelis and Zver[6] to handle quantitative photopyroelectric spectroscopy of semiconducting samples with finite thickness has been demonstrated, consistently with its earlier success in analyzing thin film spectra. The main results of our study can be summarized as follows: (1) the dual-channel (real-time normalizing) photopyroelectric spectrometer has been shown to be an excellent instrument for non-destructive evaluation of semiconductors of arbitrary thickness. (2) For the first time, the possibility of extracting the optical-absorption-coefficient and the non-radiative quantum efficiency spectra by using only one experimental photopyroelectric spectrum at only one modulation frequency has been demonstrated. This can be attained by use of the in-phase and quadrature channels of the output normalized photopyroelectric signal. (3) Simple, simultaneous spectroscopic measurements of the optical absorption coefficient and non-radiative quantum efficiency spectra of *c*-Si have been obtained. The former are limited in the opaque region by photopyroelectric saturation.

ACKNOWLEDGEMENTS

The support of the Ontario Laser and Lightwave Research Center (OLLRC) and the Natural Sciences and Engineering Research Council of Canada (NSERC), which made this work possible, are gratefully acknowledged.

REFERENCES

1. H. Coufal and A. Mandelis, in *Photoacoustic and Thermal Wave Phenomena in Semiconductors*, Edited by A. Mandelis (North-Holland, New York, 1987) p. 149.
2. C. Christofides, K. Ghandi and A. Mandelis, *Meas. Sci. Technol.*, **1**, 1363 (1990).
3. C. Christofides and A. Mandelis, Infrared Differential Photopyroelectric Spectroscopy on Crystalline Semiconductors, 36th Canadian Spectroscopic Conference, St. Catherines, Ont, Canada (August 1–3, 1990).
4. A. Mandelis, R. E. Wagner, K. Ghandi, R. Baltman and P. Dao, *Phys. Rev. B*, **39**, 5204 (1989).

5. C. Christofides, A. Mandelis, K. Ghandi and R. E. Wagner, *Rev. Sci. Instrum.*, **61,** 2360 (1990).
6. A. Mandelis and M. M. Zver, *J. Appl. Phys.*, **57,** 4421 (1985).
7. A. Mandelis, W. L. Lo and R. Wagner, *Appl. Phys.*, **A44,** 123 (1987).
8. S. M. Sze, *Physics of Semiconductor Devices* (Wiley-Interscience, New York, 1969) ch. 2.
9. Y. S. Touloukian, P. W. Powell, C. Y. Ho and M. C. Nicolaou, in *Thermophysical Properties of Matter,* Vol. 10 (IFI/Plenum, New York, Washington, 1973) p. 160.
10. P. Kirev, *The Physics of Semiconductors,* (Mir, Moscow, 1975) ch. 8.
11. Y. Dupin, Z. Angru, W. Zhaoyong, *J. Phys. D.*, **21,** 641 (1988).
12. M. Kitamura, T. Ogawa and T. Arai, *J. Phys. Soc., Japan,* **52,** 2561 (1983).
13. D. Cahen, *Appl. Phys. Lett.*, **33,** 810 (1978).